JGS
Journal of the Geological Society

Research article

Published online September 9, 2015

doi:10.1144/jgs2014-114 | Vol. 173 | 2016 | pp. 228–239

Re-evaluating the geochronology of the Permian Tarim magmatic province: implications for temporal evolution of magmatism

Shimai Shangguan[1, 2, 3*], Ingrid Ukstins Peate[3], Wei Tian[4] & Yigang Xu[1]

[1] State Key Laboratory of Isotope Geochemistry, Guangzhou Institute of Geochemistry, Chinese Academy of Sciences, Guangzhou 510640, PR China
[2] University of Chinese Academy of Sciences, Beijing 100049, PR China
[3] Department of Earth and Environmental Sciences, University of Iowa, 115 Trowbridge Hall, Iowa City, IA 52242, USA
[4] Key Laboratory of Orogenic Belts and Crustal Evolution, MOE, School of Earth and Space Sciences, Peking University, Beijing 100871, PR China
* Correspondence: shangguanshimai@gmail.com

Abstract: The Permian Tarim magmatic province has 118 published ages, ranging from 358 to 205 Ma, but the timing of mafic magmatism is not well constrained. We report two new secondary ion mass spectrometry U–Pb zircon dates on the Halahatang trachydacite and Wajilitag olivine clinopyroxenite, which are 287.2 ± 2.0 Ma and 283.2 ± 2.0 Ma, respectively. The trachydacite overlies the uppermost basalt and constrains the latest eruption age of basalt in northern Tarim. The latter is the first high-resolution date for the Wajilitag mafic layered intrusion. By screening all published ages, we identified 22 robust ages, ranging from 290.9 ± 4.1 to 261.7 ± 1.8 Ma. The robust ages together with our new data reveal a protracted period of mafic magmatism at *c*. 283 and *c*. 267 Ma. Silicic magmatism occurred from 291 to 272 Ma. Although the current known volume of Tarim basalt is too small to qualify as a large igneous province, the eroded and intrusive components, as well as pyroclastic deposits and silicic lavas, may increase the estimated volume. Further work is required to refine the duration of magmatism and the volume estimate of the province.

Supplementary material: A list of all the published dates, raw data of published ^{40}Ar–^{39}Ar dates, raw data of published U–Pb dates, published geochemistry data used for calculation and complete details of the data evaluation are available at http://www.geolsoc.org.uk/SUP18862.

Received 3 October 2014; **revised** 2 July 2015; **accepted** 2 July 2015

Extensive Permian magmatism is found in the Tarim Basin in NW China (Fig. 1), and many researchers have interpreted it to represent a large igneous province (LIP) based on the area of volcanic rocks exposed in outcrop and found in drill cores (e.g. Yang *et al.* 2007; Tian *et al.* 2010; Xu *et al.* 2014). The magmatism can be divided into two main components (Fig. 1): (1) extrusive rocks, consisting of basaltic, andesitic, dacitic and rhyolitic lavas, and mafic and silicic pyroclastic deposits; (2) intrusive rocks, including mafic–ultramafic layered intrusions, syenite intrusion, mafic and silicic dykes, ultramafic breccia pipes and granite intrusions (e.g. C.L. Zhang *et al.* 2008, 2010; Tian *et al.* 2010; Wei & Xu 2011, 2013; Yu *et al.* 2011*b*; and references therein).

The details of the temporal evolution of Tarim magmatism are poorly constrained, despite the large number of geochronological studies available. There are 118 published geochronology dates on Tarim magmatism, on a wide range of lithological units by many techniques (whole-rock K–Ar, whole-rock ^{40}Ar–^{39}Ar, mineral ^{40}Ar–^{39}Ar, mineral U–Pb dates by laser ablation inductively coupled plasma mass spectrometry (LA-ICP-MS), secondary ion mass spectrometry (SIMS), sensitive high-resolution ion microprobe (SHRIMP) and chemical abrasion thermal ionization mass spectrometry (CA-TIMS), whole-rock Rb–Sr and whole-rock Sm–Nd), which range from 358 to 205 Ma, with a span of 153 myr (Fig. 2a and b). Flood basalts, the most significant extrusive component, have an age range from 297.4 ± 5.6 Ma (basalt zircon U–Pb date, Zhang *et al.* 2012) to 252.3 ± 3.5 Ma (whole-rock ^{40}Ar–^{39}Ar date, Liu *et al.* 2012), a 45 myr time span. Whether this large time period represents a continuum or distinct multiple pulses of magmatism, or simply issues with the geochronology results, is not clear. This raises questions about whether the Tarim meets the classification of a large igneous province (LIP), defined by Ernst (2014) as emplacing substantial amounts of mafic magma (areal extent >0.1 Mkm^2 and igneous volume >0.1 Mkm^3) within a short duration pulse or multiple pulses (less than 1–5 myr), with a maximum lifespan of up to 50 myr. Published geochronological data are often taken at face value without careful consideration of their reliability or whether the geological context of the sample is known. There have been some previous efforts to re-evaluate published geochronology results (e.g. Li *et al.* 2011; Wei *et al.* 2014), but on rather limited datasets. Some of the potential issues associated with data quality and validity include the following: (1) the effects of alteration on K–Ar and ^{40}Ar–^{39}Ar dates; (2) dating xenocrysts or antecrysts that may not represent the crystallization age of their host rocks (e.g. perovskite in kimberlite, zircon in basalt). Thus, it is appropriate to comprehensively re-evaluate the previous geochronology work, and also to carry out new geochronology studies on samples selected to answer specific issues with the Tarim magmatism chronology.

This paper addresses both of these issues by providing two new SIMS U–Pb zircon ages on a trachydacite lava from Halahatang and an olivine clinopyroxenite from the Wajilitag mafic–ultramafic layered intrusion, and a comprehensive re-evaluation of the published ages. The trachydacite sample was chosen as it overlies the uppermost basalt lavas in the Halahatang region (Fig. 3a), and thus

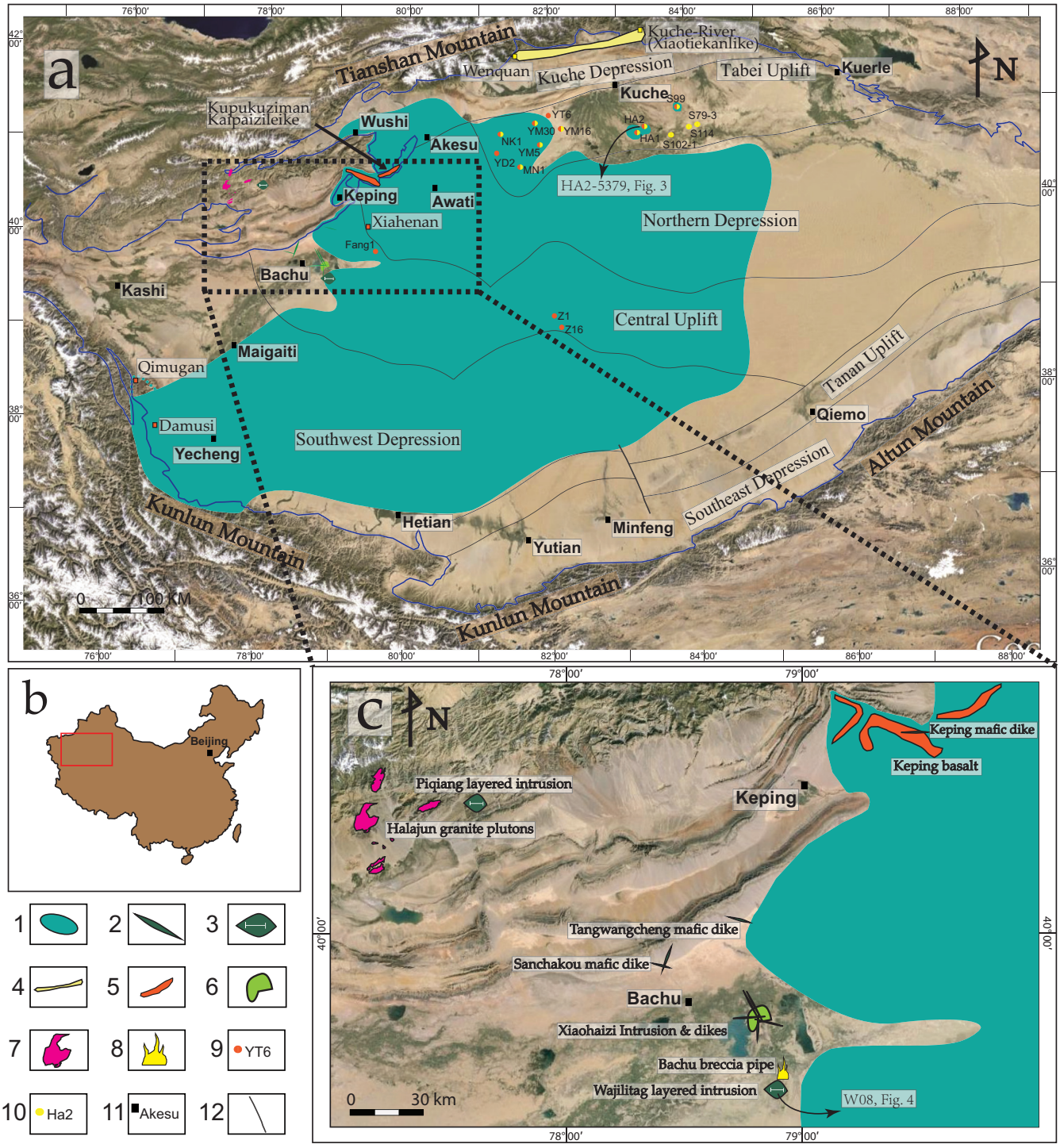

Fig. 1. (**a**) Geological map of the Tarim basin, showing the distribution of Permian magmatism (modified after Tian *et al.* 2010). (**b**) Map of China to show location of the Tarim Basin (square). (**c**) Detailed geological map of NW Tarim. 1, Inferred extent of subsurface basalt lavas (Pan 2011); 2, mafic dyke (not to scale); 3, layered intrusion; 4, rhyolite outcrop; 5, basalt outcrop; 6, syenite body; 7, granite pluton; 8, breccia pipe (not to scale); 9, drill well with basalt; 10, drill well with rhyolite (dacite); 11, city (town); 12, fault.

constrains the age of the youngest mafic volcanism in this area. The age of the mafic intrusive component of Tarim magmatism and its temporal relationship to the extrusive magmatism is not well constrained either (Fig. 2b). Therefore, the olivine clinopyroxenite sample was analysed to provide the first high-resolution date for the Wajilitag mafic–ultramafic layered intrusion. By carefully examining sample locations, experimental procedures and data interpretation, combined with both the established and newly developed evaluation approaches for geochronology data, we have identified a subset of 22 previously published ages that we consider to be robust (Fig. 2c). These high-quality ages, combined with the two new ages, are then used to develop a revised model for the temporal evolution of magmatism in the Tarim during the Permian.

Geological background

Bounded by the Tianshan Mountains to the north and NW, the Kunlun Mountains to the SW and Altun Mountains to the SE (Fig. 2a), the Tarim Basin is located in northwestern China and occupies an area of *c.* 600 000 km^2 (Xu *et al.* 2014). The floor of

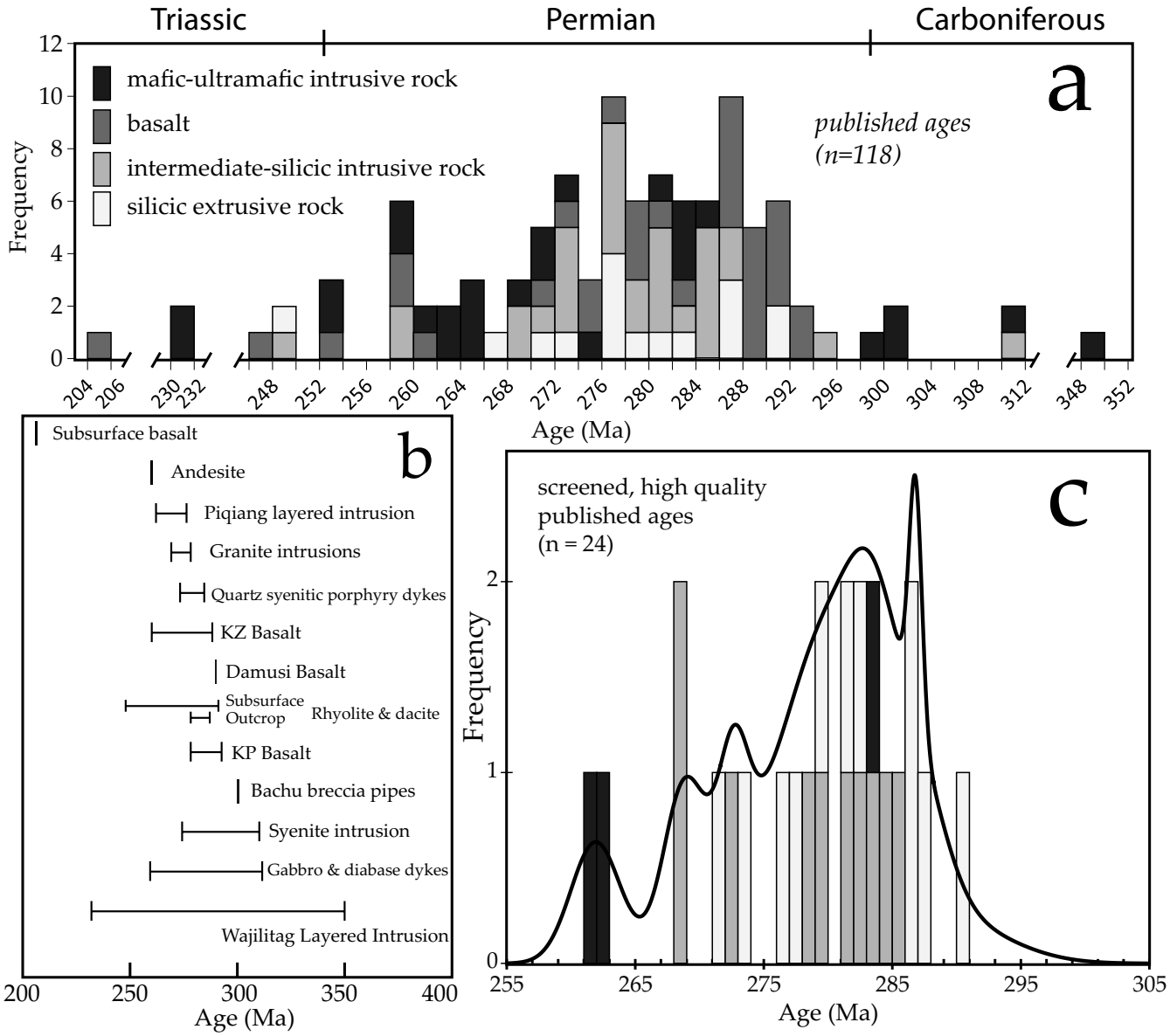

Fig. 2. (**a**) Histogram of published ages for 'Permian' magmatism in the Tarim Basin, divided into different rock types. (**b**) Published age spans of the main rock units in the Tarim Basin. (**c**) Histogram and probability density plot of 24 published ages, inferred to be of high quality (see text for details; symbol key same as for (**a**)), and excluding the detrital zircon maximum depositional age. KP, Kupukuziman Formation; KZ, Kaipaizileike Formation.

the basin is a complex Precambrian basement, which is believed to be a fragment of the Rodinian supercontinent (Li *et al.* 2003; Lu *et al.* 2008) and is overlain by thick sequences of Ordovician, Permian and Cretaceous strata (Jia 1997; Zhang 2003). A large volume of Permian extrusive rocks, including flood basalt and rhyolite lavas, as well as mafic–ultramafic intrusive complexes and mafic dykes are widely reported in the Tarim Basin (e.g. Jia 1997; Yang *et al.* 2006, 2007; Fig. 1).

Subsurface seismic and drilling data indicate that the Tarim basalt lavas have an estimated areal extent of 265 000 km^2 and a volume of 40 000 km^3 (Pan 2011; Pan *et al.* 2013; Fig. 2). The distribution of outcrop and subsurface data suggests that the bulk of the province (>99%) is covered by the Taklamakan Desert sands and Quaternary sediments (Fig. 1a). The main outcrop of flood basalt is located in Keping, which exposes *c*. 100 km of lateral section (Fig. 1c), and a cumulative thickness of *c*. 400 m. The Keping outcrop consists of two packages of basaltic lavas and volcaniclastic rocks with a *c*. 800 m sedimentary package between them. The lower basalts and intercalated clastic deposits are called the Kupukuziman Formation, and the upper basalts and intercalated clastic deposits are called the Kaipaizileike Formation. The thick intermediate unit has not been formally described, but is informally referred to as the FP Formation (Shangguan *et al.* 2012). Other smaller basalt outcrops have been reported from the Damusi and Qimugan (Yang *et al*. 2006; Li *et al.* 2013). Thick sequences of subsurface basalt lavas (>1200 m) were also reported from drilling data in northern Tarim (Tian *et al.* 2010). Felsic lavas have limited exposures in the Xiaotiekanlike–Wenquan outcrop (Liu *et al.* 2014), and multiple felsic lava layers are also reported coexisting with the basalts from drilling data in northern Tarim (Tian *et al.* 2010). Intrusive complexes, including the Wajilitag and the Piqiang mafic–ultramafic intrusions, the Xiaohaizi syenite body and the Piqiang granites are all located around the NW margin of the basin (e.g. Wei & Xu 2013; Zhang & Zou 2013). Owing to the lack of seismic data, the actual dimensions of the intrusive complexes are still unclear. Mafic dykes are widespread in the Bachu area and Keping, and some intrude the syenite body and the Keping basalt. The thickness of Bachu dykes ranges from 0.6 to 4 m (Z.L. Zhang *et al.* 2008), and the Keping dykes have a mean thickness of 3.8 m (Chen *et al.* 2014). Finally, kimberlite breccia pipes and dykes have been reported in the Wajilitag region (e.g. Li *et al.* 2010; Zhang *et al.* 2013), but no geochemical or field contact

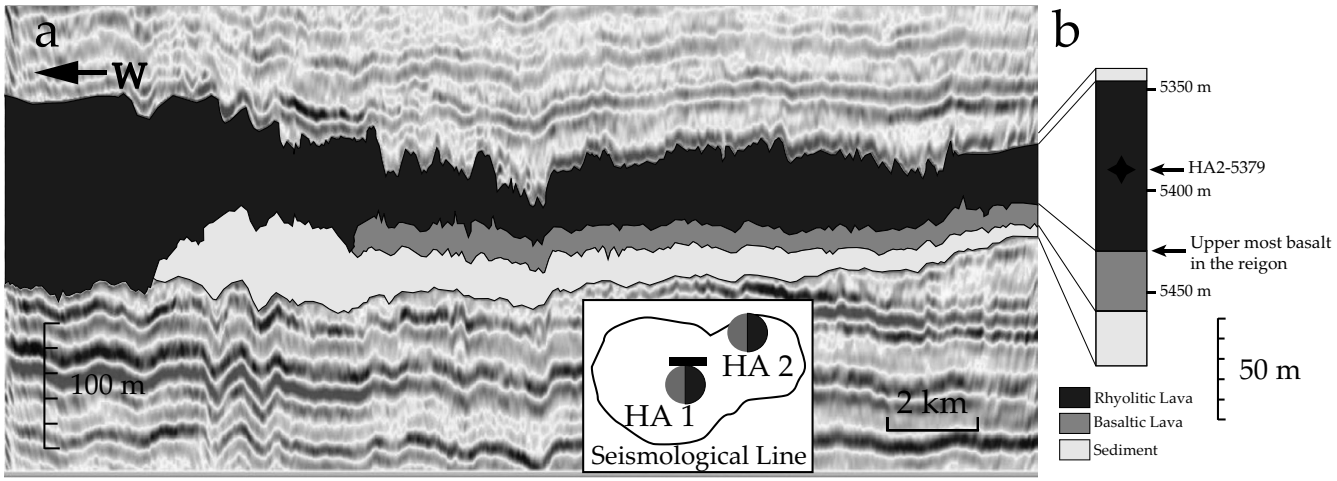

Fig. 3. (**a**) Seismic cross-section of HA2 well and adjacent area (China National Petroleum Corporation, pers. comm. 2013); inset shows the location of the seismic line. (**b**) Stratigraphic column of HA2 well located at 41°20'01"N, 83°20'45"E.

relationships have been observed between the breccia pipes (dykes) and the Wajilitag intrusion.

Sample locations

In the Halahatang area, located in the eastern part of the Northern Tarim Uplift (Fig. 1a), Permian extrusive magmatism is found only in the subsurface, as revealed through drilling and seismic data. The total thickness of basalt lavas varies from 30 to 300 m, thinning from SW to NE. Four lithological units are identified in the Halahatang 2 drill well (HA2, global positioning system (GPS) coordinates 41°20'01"N, 83°20'45"E): (1) epiclastic sediment (5460–5485 m); (2) basalt lava (5430–5460 m); (3) trachydacite lava (5345–5430 m); (4) sediment (5345 m to surface) (Fig. 3). A seismic reflection project (Fig. 3a) shows that the trachydacite layer extends for at least 23 km laterally. The trachydacite drill core sample HA2-5379 chosen for SIMS dating was collected from 5379 m depth in the HA2 well (Fig. 3b). The sample is dense, massive and fresh, with porphyritic texture. The phenocrysts are composed of 30–35 vol% alkali feldspar and 5–10 vol% quartz, and the matrix is fine-grained alkali feldspar, quartz and biotite.

The Wajilitag layered intrusion is located to the SE of the Bachu County, *c*. 25 km away from the Xiaohaizi syenite intrusion (Fig. 4). The layered intrusion cuts Silurian and Devonian strata and hosts economic Fe–Ti oxide mineralization (C.L. Zhang *et al.* 2008; Cao *et al.* 2013), consistent with strong aeromagnetic anomalies in the Piqiang, Bachu and Aksu regions (Rui *et al.* 2002). The Wajilitag layered intrusion and the Xiaohaizi syenite intrusion have been interpreted as constituents of a larger layered intrusion (C.L. Zhang *et al.* 2008; Cao *et al.* 2013), but this interpretation needs to be confirmed by seismic data (Zhou *et al.* 2009). The outcrop of Wajilitag layered intrusion is 5 km long, 1.5–3 km wide and 100–300 m thick (Gao 2007), with contact zones dipping 20–40° toward the interior of the complex (C.L. Zhang *et al.* 2008). The layered intrusion is divided into four main lithofacies: (1) olivine-clinopyroxenite; (2) pyroxenite; (3) gabbro; (4) syenite and quartz syenite (Fig. 4; Li *et al.* 2001; C.L. Zhang *et al.* 2008; Cao *et al.* 2013). The olivine clinopyroxenite sample (W08) selected for SIMS dating was collected from the middle part of the layered intrusion (GPS coordinates 39°31'57"N, 78°56'03"E, Fig. 4). The sample is composed of 45–55 vol% clinopyroxene, 10–15 vol% olivine, 10–20 vol% plagioclase and 5–10 vol% Fe–Ti oxides, with minor apatite.

Analytical procedures

Zircon crystals were extracted from HA2-5379 and W08 by density and magnetic separation, and selected grains were handpicked for analysis. Zircons were mounted in epoxy together with the standard Plesovice zircon (Sláma *et al.* 2008) and polished. Cathodoluminescence (CL) and transmitted and reflected light images of all zircons were obtained to guide SIMS U–Pb measurement. CL images were obtained using a FEI PHILIPS XL30 scanning electron microscope in Peking University, with analytical conditions of 12 kV and 12 μA.

U–Pb ages were measured by SIMS at the State Key Laboratory of Lithospheric Evolution, Institute of Geology and Geophysics, Chinese Academy of Sciences. Zircon analytical procedures by SIMS follow those of Li *et al.* (2009). The measured Pb isotopic compositions were corrected for common Pb using non-radiogenic ^{204}Pb. Corrections were small enough to be insensitive to the choice for the common Pb composition. An average of present-day crustal compositions (Stacey & Kramers 1975; Wiedenbeck *et al.* 1995) was used for the common Pb. Data processing was done using the Isoplot 3.6 software (Ludwig 2008). Errors of single analyses are quoted for 1σ uncertainty. Ages are quoted as weighted mean values at 95% confidence levels.

Analytical results

Halahatang trachydacite (HA2-5379)

A total of 18 spot analyses were obtained (Table 1). Zircon grains are euhedral cylindrical, with lengths of 50–150 μm and a length/width ratio of 4:1 to 1.5:1 (Fig. 5), and show clear and dense concentric zoning. Th/U ratios range from 0.48 to 0.89, with U contents of 57–167 ppm, which indicate a typical magmatic origin. On the $^{206}Pb/^{238}U$–$^{207}Pb/^{235}U$ concordia plot, we eliminated one analysis (analysis 4), which plots away from the concordant line. The apparent $^{206}Pb/^{238}U$ ages of the remaining 17 concordant analyses (Fig. 6) lie between 293.3 and 281.3 Ma, yielding a weighted mean $^{206}Pb/^{238}U$ age of 287.3 ± 2.0 Ma (MSWD = 0.91, probability = 0.61) that is interpreted as the timing of trachydacite emplacement.

Wajilitag olivine-clinopyroxenite (W08)

A total of 19 spot analyses were obtained (Table 2). Zircon grains show magmatically resorbed textures, with lengths of 50–150 μm and a length/width ratio of 1:1 to 2:1 (Fig. 5). They have dense zoning, Th/U ratios from 0.97 to 2.39, and U contents from 57 to 167 ppm, indicating a typical magmatic origin. On the $^{206}Pb/^{238}U$–$^{207}Pb/^{235}U$ concordia plot, 17 of the 19 analyses are concordant (analyses 6 and 7 fall off concordant line and cannot be used) (Fig. 6). The apparent $^{206}Pb/^{238}U$ age of the concordant analyses lie between 286.9 and 279.2 Ma, yielding a weighted mean $^{206}Pb/^{238}U$

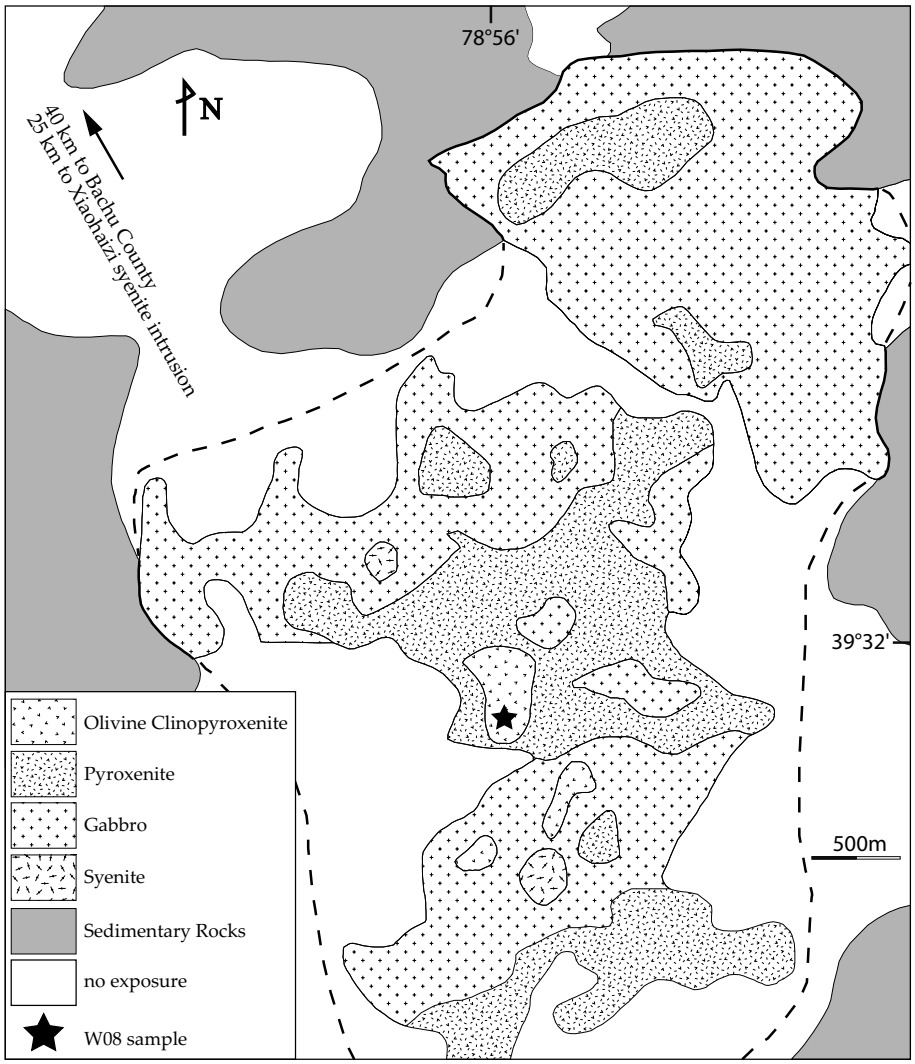

Fig. 4. Geological map of the Wajilitag complex (modified from C.L. Zhang *et al.* 2008 and Cao *et al.* 2013). Location of W08 sample is 39°31'57"N, 78°56'03"E.

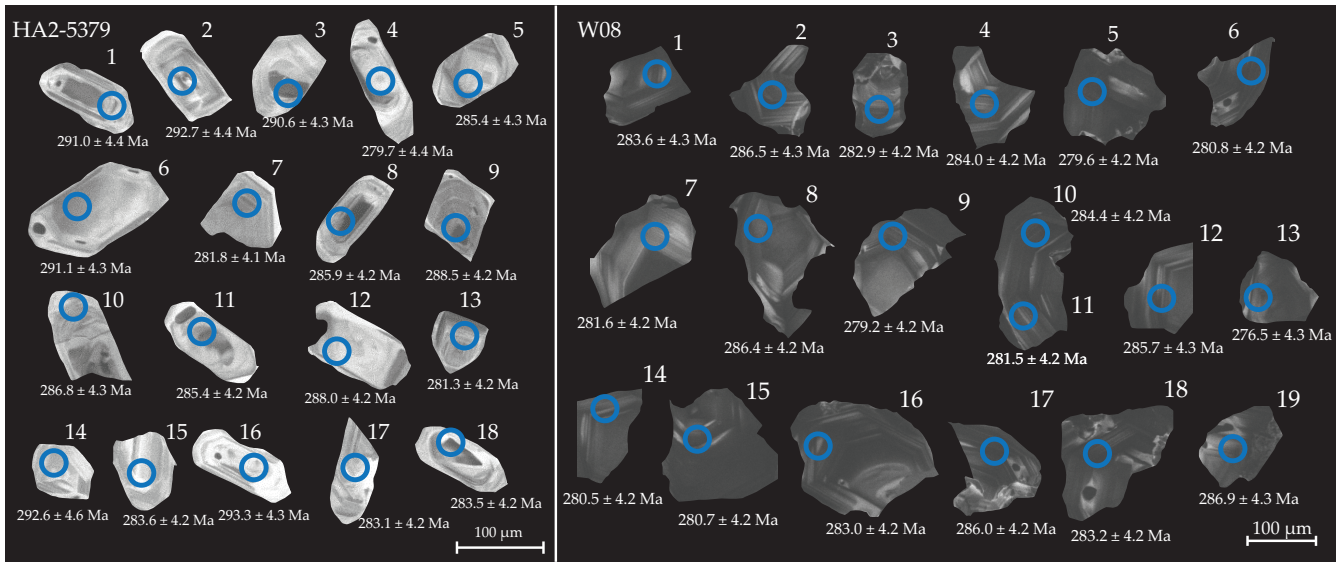

Fig. 5. Cathodoluminescence (CL) images of all the zircons from sample HA2-5379 and W08. The spot positions and corresponding ages are marked.

age of 283.2±2.0 Ma (MSWD=0.36, probability=0.991). Based on the similarity of zircon textures and narrow distribution of single-grain ages, we interpret this age as a good indication of the crystallization age of the olivine clinopyroxenite.

Re-evaluation of published geochronological data

Since 1991, 118 ages of Permian Tarim mafic and silicic magmatism have been reported. Unfortunately, not all of these published ages present adequate information on geological context or raw

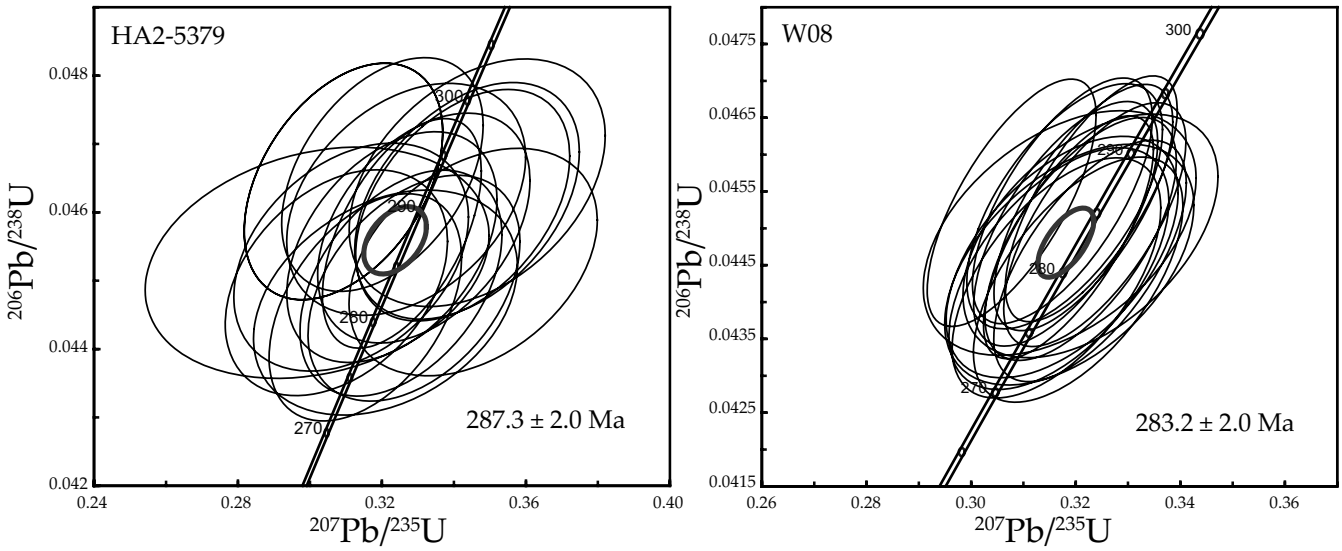

Fig. 6. U–Pb concordia diagram for zircons from HA2-5379 and W08.

Table 1. *SIMS zircon U–Pb isotopic data and calculated apparent ages of HA2-5379*

Spot	U (ppm)	Th (ppm)	Th/U	f^{206}Pb (%)	^{207}Pb/^{235}U	±1σ (%)	^{206}Pb/^{238}U	±1σ (%)	Rho	^{207}Pb/^{206}Pb	±1σ (%)	$t_{206/238}$ (Ma)	±1σ (Ma)
HA2@1	73	59	0.81	0.23	0.34364	3.71	0.0462	1.53	0.413	0.05398	3.38	291	4.4
HA2@2	98	84	0.86	0.22	0.30932	3.64	0.0465	1.52	0.418	0.0483	3.31	292.7	4.4
HA2@3	82	50	0.62	0.37	0.34245	3.54	0.0461	1.5	0.423	0.05387	3.21	290.6	4.3
HA2@4	74	44	0.59	0	0.24729	17.9	0.0443	1.62	0.091	0.04044	17.8	279.7	4.4
HA2@5	83	45	0.54	0.09	0.30198	6.46	0.0453	1.52	0.236	0.04839	6.28	285.4	4.3
HA2@6	60	36	0.61	0.25	0.32672	4.15	0.0462	1.5	0.362	0.0513	3.87	291.1	4.3
HA2@7	87	71	0.82	0.36	0.32097	4.67	0.0447	1.5	0.322	0.0521	4.42	281.8	4.1
HA2@8	62	30	0.48	0.52	0.31144	4.27	0.0453	1.5	0.351	0.04981	4	285.9	4.2
HA2@9	78	61	0.78	0.28	0.33164	3.63	0.0458	1.5	0.413	0.05255	3.31	288.5	4.2
HA2@10	79	71	0.89	0.21	0.32277	3.69	0.0455	1.51	0.41	0.05146	3.37	286.8	4.3
HA2@11	61	30	0.49	0.8	0.34534	4.08	0.0453	1.5	0.368	0.05532	3.79	285.4	4.2
HA2@12	167	100	0.6	0.16	0.32554	2.77	0.0457	1.5	0.542	0.05167	2.33	288	4.2
HA2@13	101	61	0.6	0.42	0.31539	3.46	0.0446	1.52	0.439	0.05128	3.11	281.3	4.2
HA2@14	57	43	0.75	0.25	0.34646	4.19	0.0464	1.59	0.38	0.05412	3.88	292.6	4.6
HA2@15	106	62	0.58	0	0.30734	4.1	0.045	1.5	0.365	0.04957	3.82	283.6	4.2
HA2@16	101	54	0.53	0.3	0.32014	3.57	0.0466	1.5	0.42	0.04988	3.24	293.3	4.3
HA2@17	124	76	0.61	0.18	0.32889	3.66	0.0449	1.5	0.411	0.05314	3.33	283.1	4.2
HA2@18	86	49	0.57	0.45	0.32528	3.53	0.045	1.5	0.426	0.05247	3.19	283.5	4.2

f^{206}Pb = common ^{206}Pb/total ^{206}Pb.

Table 2. *SIMS zircon U–Pb isotopic data and calculated apparent ages of W08*

Spot	U (ppm)	Th (ppm)	Th/U	f^{206}Pb (%)	^{207}Pb/^{235}U	±1σ (%)	^{206}Pb/^{238}U	±1σ (%)	Rho	^{207}Pb/^{206}Pb	±1σ (%)	$t_{206/238}$ (Ma)	±1σ (Ma)
W08@1	97	94	0.97	0.00	0.31693	3.36	0.0449	1.51	0.449	0.05115	3	283.6	4.3
W08@2	318	461	1.45	0.04	0.31745	2.21	0.0454	1.5	0.678	0.05074	1.63	286.5	4.3
W08@3	259	320	1.23	0.05	0.32094	2.33	0.0449	1.5	0.644	0.05189	1.78	282.9	4.2
W08@4	319	586	1.84	0.04	0.32364	2.2	0.0451	1.5	0.682	0.0521	1.61	284	4.2
W08@5	265	384	1.45	0.05	0.31632	2.58	0.0443	1.5	0.583	0.05176	2.09	279.6	4.2
W08@6	165	248	1.5	0.16	0.33362	2.63	0.044	1.55	0.59	0.05499	2.13	276.5	4.3
W08@7	132	200	1.52	0.18	0.30043	3.52	0.0445	1.51	0.429	0.04897	3.18	281.6	4.2
W08@8	572	1061	1.86	0.00	0.32297	2.08	0.0454	1.5	0.722	0.05159	1.44	286.4	4.2
W08@9	223	319	1.43	0.00	0.32047	2.55	0.0443	1.53	0.601	0.05246	2.04	279.2	4.2
W08@10	297	559	1.88	0.03	0.31808	2.26	0.0451	1.5	0.665	0.0512	1.69	284.4	4.2
W08@11	326	553	1.7	0.00	0.31739	2.85	0.0446	1.5	0.526	0.0516	2.43	281.5	4.2
W08@12	243	504	2.07	0.12	0.31789	2.41	0.0453	1.5	0.624	0.0509	1.88	286	4.2
W08@13	422	900	2.13	0.00	0.32274	2.33	0.0446	1.5	0.644	0.05253	1.78	280.8	4.2
W08@14	169	257	1.52	0.13	0.3168	2.71	0.0445	1.51	0.556	0.05169	2.25	280.5	4.2
W08@15	117	139	1.19	0.25	0.31876	3.05	0.0445	1.5	0.491	0.05194	2.66	280.7	4.2
W08@16	155	243	1.56	0.18	0.32281	3.09	0.0449	1.5	0.487	0.05215	2.69	283	4.2
W08@17	330	788	2.39	0.11	0.32146	2.17	0.0453	1.51	0.693	0.05149	1.57	285.7	4.3
W08@18	434	525	1.21	0.05	0.31861	2.08	0.0449	1.5	0.72	0.05149	1.45	283.2	4.2
W08@19	374	871	2.33	0.06	0.30774	2.14	0.0453	1.51	0.705	0.04922	1.52	286.9	4.3

f^{206}Pb = common ^{206}Pb/total ^{206}Pb.

data. The ages without context and/or raw data are not considered further here (a total of 35 ages). For the ages with inconsistent geological context in two or more publications, we review the data but consider the contradictory information an open problem. For the remaining ages with clear geological context and complete raw data, we carefully evaluate each age based on criteria specific to the method used and the particular rock types. Published data are assigned into four categories: group 1, highest quality data, with clear field observations, analytical method descriptions and robust statistical perspectives (Fig. 2c); group 2, data that provide chronological constraints with less precision and accuracy, owing to either inconclusive field relationship or large errors that cannot be attributed to a specific cause or sample material issues; group 3, data with large errors, discordance or RHO value (correlation coefficient; e.g. Schmitz & Schoene 2007) outside the 0–1 range; group 4, data that lack critical information (e.g. sample location, analytical methods) or raw data. Below we briefly summarize the basic approaches taken for data evaluation for the various geochronological methods, and also summarize the results for Tarim samples.

(1) ^{40}Ar–^{39}Ar dating. The $^{40}Ar/^{39}Ar$ step-heating method uses a series of apparent ages to recover possible crystallization ages for igneous rocks, and the reproducibility of the resulting step ages requires the data to meet a basic statistical hypothesis (Marzoli *et al.* 1999; Baksi 2003). Alteration in basalt lavas older than a few million years may disturb igneous whole-rock material used for argon dating (e.g. Karoo, Duncan *et al.* 1997; Deccan, Baksi 2014) and usually results in inaccurate estimates of the crystallization age (Baksi 2007*a*,*b*). Therefore statistical tests on plateau sections for validity (Baksi 2003; Sharp & Clague 2006) and the alteration state test on dating material (Baksi 2007*a*,*b*) are simultaneously applied here to evaluate the reliability of $^{40}Ar/^{39}Ar$ dates. None of the 20 ^{40}Ar–^{39}Ar dates in Tarim satisfy these statistical and alteration criteria simultaneously, and thus may not yield reliable ages.

(2) Zircons from basalt. Zircons have been found in mantle-derived basalts and dated by U–Pb methods (e.g. Katayama *et al.* 2003; Polat *et al.* 2009). The question is what the relationship between the zircon and the host basalt magma really is. Experimental petrology suggests that zircons are unlikely to crystallize directly from a basalt magma (Boehnke *et al.* 2013), and it is probable that the zircons are crustal-derived xenocrysts entrained during either ascent or emplacement on the surface. Therefore, these zircons are rarely used to represent the age of the host rock. In the case of the zircons from the Keping basalt dated by D.Y. Zhang *et al.* (2010) and Yu *et al.* (2011*b*), difference in Hf isotope compositions of the zircons and the host basalt suggests a xenocrystic origin.

(3) Silicic extrusive and intrusive rocks. Advances in zircon TIMS and SIMS analyses have revealed a protracted history of zircon crystallization prior to eruption, of potentially more than several million years, in many silicic magmatic units (e.g. Miller *et al.* 2007; Bryan *et al.* 2008). Hence, the weighted mean age of single-grain U–Pb dates will represent an average age for zircon crystallization, which can be older than the eruption or emplacement age of the host rock. To address this, we replot every date of silicic rocks to try to confirm the presence of distinct populations. The zircons from silicic extrusive rocks show age scatter to variable extent, but the continuous single-grain age distribution and the relatively low resolution of the dating technique impede further interpretation. The only TIMS dating (Liu *et al.* 2014), of which the expected precision should be better than 0.1% (Mattinson 2005), reveals distinct populations of zircon, and we take the weighted mean of the youngest age population as the best approximation of the eruption age of the host rhyolite. For the Xiaohaizi syenite intrusion, the 6.2 myr age span from different rock units could result from analytical error, but is more probably attributed to a long-lived syenitic centre. Scattered single-grain ages are also observed in granite plutons, and the extent of scatter can be linked to Zr saturation temperature.

(4) Detrital zircons. Detrital zircon ages can be used as a tool to evaluate the maximum depositional age of the host sedimentary rock (e.g. Brown & Gehrels 2007). Dickinson & Gehrels (2009) proposed four measures to infer the youngest detrital zircon ages present in a sample. They are, from least to most statistically robust, (a) youngest single-grain age (YSG), (b) youngest graphical age peak controlled by more than one grain age (YPP), (c) mean age of the youngest two or more grains that overlap in age at 1σ (YC1σ(2+)), and (d) mean age of the youngest three or more grains that overlap in age at 2σ (YC2σ(3+)). The YC2σ(3+) ages of three samples from Zou *et al* (2013) conservatively constrain the sixth, fourth and first basalt layers of the KZ basalt at Keping to be younger than 263.7 ± 3.4, 267.0 ± 3.4 and 287.6 ± 3.8 Ma, respectively. Li *et al.* (2013) gave the YC2σ(3+) age of underlying sandstone of the Damusi basalt as 284.1 ± 4.7 Ma.

(5) U–Pb dating of mafic dykes. Zircon crystallizes in a differentiated gabbroic environment and can be used to represent the crystallization age of host rock (e.g. Kaczmarek *et al.* 2008). However, zircons in a mafic environment usually experience a complex history, which makes it necessary to identify zircon origins and group populations by variable approaches such as zircon chemistry and morphology (e.g. Grimes *et al.* 2009). The U–Pb dating of single mafic dyke samples of Tarim shows a large age span (e.g. Wajilitag gabbro, Zhang *et al.* 2009), scattered single-grain age distribution (e.g. Xiaohaizi diabase, Li *et al.* 2007), a large number of discordant ages (e.g. Yijianfang diabase, Zhang *et al.* 2009) and a large portion of xenocrystic zircons (e.g. Xiaohaizi diabase, Wei & Xu 2013). All these issues hinder a proper interpretation of previous mafic dyke dates. Furthermore, the geographically isolated dykes are used as a horizontal marker in Tarim, to chronologically relate different rock units (Li *et al.* 2011; Yang *et al.* 2013). LIP-related dyke swarms usually have an average thickness >10 m (Ernst *et al.* 1995) and maximum thickness >70 m (Abbott & Isley 2002), and may have extents greater than 1000 km (Ernst 2014). The Keping dykes are the thickest in Tarim, and have an average thickness of 3.8 m, maximum thickness of 21.4 m and maximum exposed length of 17.1 km (Chen *et al.* 2014), which are significantly smaller in dimension compared with typical LIP-related dyke swarms. Thus the dykes found in Tarim cannot be used as a horizontal marker.

(6) Kimberlite mineral U–Pb dating. Perovskite and baddeleyite from kimberlitic rocks commonly show significant compositional heterogeneity (e.g. Heaman 1989; Heaman & Kjarsgaard 2000; Sarkar *et al.* 2011; Schärer *et al.* 2011). Kimberlite eruptions can be characterized by multiple pulses sharing the same magma conduit and entrain xenocrystic material at depths throughout the lithosphere (Sparks 2013). Therefore, perovskites and baddeleyites may belong to different generations, and may not define the kimberlite eruption age. Different perovskite and baddeleyite populations may be recognized by differences in size, morphology and composition (e.g. Sarkar *et al.* 2011; Schärer *et al.* 2011), and presumably on a weighted mean U–Pb age plot. The assumption that dated perovskites are cogenetic with the host kimberlite can also be tested using partition coefficient data from Beyer *et al.* (2013) to calculate melt compositions in equilibrium with the perovskites. In the study by Zhang *et al.* (2013), the large diversity of Th concentrations and large age span among single grains of both perovskite and baddeleyite, and the disequilibrium condition between dated perovskites and the Bachu kimberlite, as well as age clusters of baddeleyites, hinder a proper interpretation of these U–Pb ages.

In summary, 24 ages are highest quality, including our two new U–Pb SIMS ages (group 1; Fig. 2c; Table 3), 12 can be used for reference (group 2), and nine data have significant errors (group 3).

Discussion

Re-evaluation of the temporal evolution of Permian Tarim magmatism

Several temporal evolution models for Tarim magmatism have been proposed by researchers (e.g. Li *et al.* 2011; Xu *et al.* 2014). Based on 27 published dates, Xu *et al.* (2014) proposed that the Permian Tarim magmatism comprises three main episodes: *c.* 300 Ma kimberlites, *c.* 290 Ma flood basalts and *c.* 280 Ma ultramafic–mafic–felsic intrusions and dyke swarms. The first episode is defined by three SIMS dates on perovskite and baddeleyite (Zhang *et al.* 2013), which we conclude here are not robust. The second episode is defined by ^{40}Ar–^{39}Ar dates (e.g. Yang *et al.* 2006; Wei *et al.* 2014) and basalt zircon dates (e.g. Yu *et al.* 2011*b*), which were not statistically robust and lack clear geochronological significance, respectively. The third episode, consisting of ultramafic–mafic–felsic intrusions and a dyke swarm, is defined by 13 ages. The mafic dykes lack reliable age information, and the robust ages of granitic plutons, syenite intrusion, silicic dykes and ultramafic intrusions yield a >20 myr time span from 285.6 ± 3.6 Ma (Sun *et al.* 2008) to 261.7 ± 1.8 Ma (Zhang & Zou 2013). Based on our new ages and reassessment of a larger database of published ages (summarized in Fig. 2), this model for the temporal evolution of Permian Tarim magmatism needs to be re-evaluated.

New ages reveal the pulsed nature of mafic magmatism

The most critical problem in establishing a temporal model for Permian Tarim magmatism is the poor age constraints on the flood basalt and mafic intrusive rocks. The Halahatang trachydacite layer we dated directly overlies the uppermost basalt in the drill core, and provides a robust constraint on the minimum emplacement age (287.2 ± 2.0 Ma) of the basalt flows in northern Tarim. Our revised interpretations of published detrital zircon data provide reliable constraints on the maximum depositional age of the host sandstone and in turn restrict the maximum emplacement age of the upper part of the Keping basalt and Qimugan basalt, which overlie the sandstones, to 267.0 ± 3.4 Ma and 284.1 ± 4.7 Ma, respectively. Thus, the basalt in Halahatang is temporally distinct from the upper part of the KZ basalt at Keping, which indicates a minimum of *c.* 20 myr time gap between basalt eruptions. This is further supported by petrochemically distinct basalts from Halahatang, Keping and Qimugan (Shangguan 2015), and they probably represent different pulses of basalt eruptions.

The Wajilitag layered intrusion has trace element patterns and εNd(t) values indicating an ocean island basalt (OIB)-like, asthenospheric mantle source, and it is similar to the Bachu mafic dykes but compositionally distinct from the Keping basalts (Cao *et al.* 2013). The new U–Pb age of 283.2 ± 2.0 Ma is a good estimate of its emplacement age. The Piqiang ultramafic–mafic complex, 150 km NW of the Wajilitag layered intrusion, was emplaced at 262.3 ± 2.1 Ma (Zhang & Zou 2013), which is *c.* 21 myr later than the Wajilitag layered intrusion. Thus the two mafic–ultramafic intrusions also represent distinct magmatic pulses and are evidence for a protracted magmatic history in the Tarim Basin. Although such large mafic layered intrusions are generally inferred to be part of the plumbing system of an LIP (e.g. Cawthorn 1996), the comagmatic volcanic piles of these two intrusions have yet to be identified.

The temporally and compositionally distinct episodes of basalt eruption and mafic–ultramafic intrusion emplacement rule out the possibility of a continuous activity of the Tarim magmatism (Fig. 7). Refining the comprehensive temporal history and chemical relationship needs to be further explored though more detailed geochronological and geochemical studies. There are many examples of LIPs that show distinct pulses of magmatic activity; in particular, those with broad age ranges (e.g. >20 myr) were usually emplaced in multiple shorter duration pluses of *c.* 1–5 Ma rather than as a continuous longer-lasting magmatic event (e.g. Courtillot & Renne 2003; Prokoph *et al.* 2004; Bryan & Ernst 2008). The North Atlantic LIP shows an initial magmatic pulse at *c.* 60 Ma and a second magmatic pulse at *c.* 55 Ma (e.g. Saunders *et al.* 1997). Another example of a multiple pulse event is the protracted Matachewan LIP with ages of *c.* 2490, 2475 and 2446 Ma, represented by dyke swarms, layered intrusions and volcanic rocks, respectively (event 206 of Ernst & Buchan 2002). Our two new ages (287.2 ± 2.0 and 283.2 ± 2.0 Ma) overlap with a probability of 31.7%, which indicates that the Halahatang basalt and the Wajilitag layered intrusion may have been emplaced at the same time. With the age constraints of critical units, at least two mafic magmatic pulses can be recognized in the Tarim province: (1) the Halahatang basalt (>287.2 ± 2.0 Ma) and Wajilitag layered intrusion (283.2 ± 2.0 Ma); (2) the upper KZ basalt (<267.0 ± 3.4 Ma) and Piqiang complex (267.0 ± 3.4 Ma) (Fig. 7). Although the ages of these pulses may overlap slightly, they can also be differentiated by separate geographical location of magmatism and different chemical composition (Shangguan 2015). Determination of the duration of the Tarim province requires additional high-resolution geochronological studies, which may subdivide the currently identified pulses, fill the gaps between pulses, or broaden the currently recognized age span of magmatism.

The temporal evolution of silicic magmatism

There are 11 robust ages on silicic extrusive rocks, which are exposed in the northern margin and buried in northern Tarim. They are evenly distributed from 290.9 ± 4.1 Ma (YM30-1, Tian *et al.* 2010) to 271.7 ± 2.2 Ma (MN1-1, Tian *et al.* 2010). Three samples (HA-5379, 287.2 ± 2.0 Ma, this paper; YM30-1, 290.9 ± 4.1 Ma, and YM 5-8, 286.6 ± 3.3 Ma, Tian *et al.* 2010) are intercalated with basaltic lavas. Eight others are not coexistent with the basalt, and range from 286.8 ± 0.5 to 271.7 ± 2.2 Ma (Fig. 7). Silicic volcanism accompanies the first pulse of mafic volcanism in northern Tarim, and continued for at least 20 myr (Fig. 7). The eight samples that are not coexistent with the basalt and are broadly distributed in northern Tarim reasonably indicate that mafic volcanism is absent in the whole northern Tarim after *c.* 287 Ma.

The syenite–granite intrusions are located at the NW periphery of the Tarim magmatic province. Four ages, on different units within the Xiaohaizi syenite body, range from 285.2 ± 3.6 to 279.7 ± 2.0 Ma, and show a positive correlation with SiO_2 content, indicating a long-lived syenitic centre. Ages on four granitic plutons range from 274.6 ± 2.2 Ma (Halajun 1, C.L. Zhang *et al.* 2010) to 268.6 ± 2.0 Ma (Halajun 3, Zhang & Zou 2013), and do not overlap in age with the syenite intrusion (Fig. 7). Studies have shown that LIP-related syenitic complexes can have significant age spans of *c.* 10 myr (e.g. Kangerlussuaq Alkaline Complex, Greenland, Riishuus *et al.* 2006), and the timeframe of granitic pluton assembly is potentially several million years (e.g. >5 myr for Mt. Stuart, WA, USA; >8 myr for Tuolumne, CA, USA; Miller *et al.* 2007). Thus, the age ranges observed here probably reflect a protracted magmatic history. The syenite and granite plutons represent two discrete, episodic phases of magmatism, at *c.* 285–280 Ma and *c.* 275–269 Ma, respectively (Fig. 7). The silicic intrusive rocks are roughly synchronous with the extrusive silicic rocks, with some older ages found in extrusive silicic units (Fig. 7). Silicic igneous

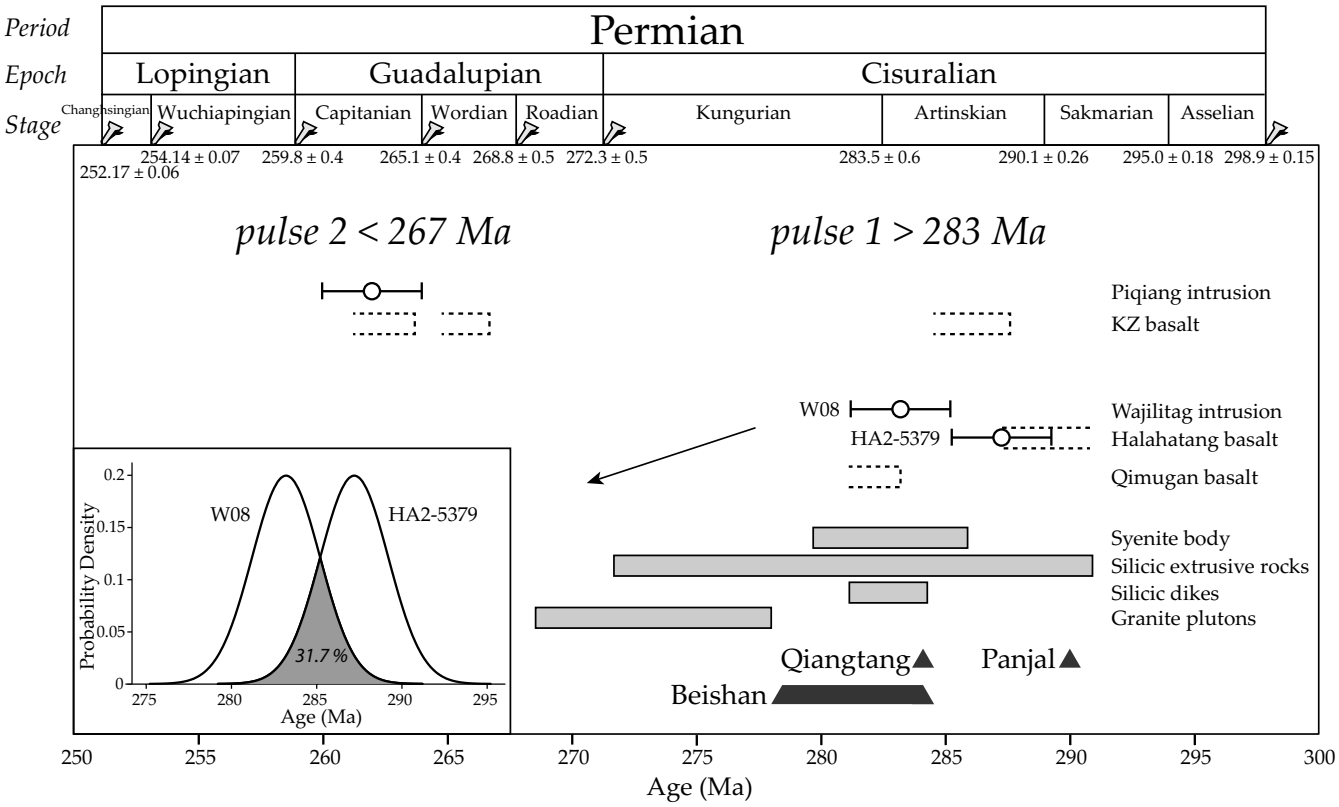

Fig. 7. Revised temporal distribution of the high-quality data for Tarim volcanism, filled bars for igneous rock geochronology; dashed-outline bars for sandstone detrital zircon geochronology. Permian time scale for reference (Cohen *et al*. 2013). Inset in the lower left corner shows the probability density plot of the two new ages. It should be noted that the two ages overlap with a probability of 31.7%.

Table 3. *Revised table for 24 high-quality ages (including two new ages)*

Section	Age (Ma)	Lithology	Method	Source	Recalculation	*n*	MSWD
Halahatang	287.2±2.0	Trachydacite	SIMS	This paper		17	0.87
Nanka 1	277.3±2.5	Rhyolite	SHRIMP	Tian *et al.* 2010	277.3±2.5	11	1.5
S102-1	281.0±3.0	Dacite	LA-ICP-MS	Yu *et al.* 2011*a*	281.0±3.0	16	2.1
S114	276.6±2.7	Dacite	LA-ICP-MS	Yu *et al.* 2011*a*	276.6±2.7	19	3.3
S79-3	279.6±3.0	Dacite	LA-ICP-MS	Yu *et al.* 2011*a*	279.6±3.0	15	1.6
S99	273.7±3.2	Dacite	LA-ICP-MS	Yu *et al.* 2011*a*	273.7±3.2	17	1.09
Wenquan	286.8±0.5	Rhyolite	CA-TIMS	Liu *et al.* 2014	284.20±1.60	4	0.074
Xiaohaizi	281.2±3.7	K-feldspar-granite vein	LA-ICP-MS	Sun *et al.* 2009	282.0±3.7	11	1.8
Xiaohaizi	284.3±2.8	Quartz syenitic porphyry	SHRIMP	Li *et al.* 2011	282.6±2.2	20	1.05
Xiaohaizi	279.7±2.0	Syenite body	SIMS	Wei & Xu 2011	279.7±2.0	18	0.26
Xiaohaizi	285.9±2.6	Syenite body	SHRIMP	Sun *et al.* 2008	285.2±3.6	15	1.4
Xiaohaizi	282±3	Syenite body	LA-ICP-MS	Li *et al.* 2007	282.4±2.7	30	2.8
Xiaohaizi	283.3±1.8	Pyroxene syenite	LA-ICP-MS	Sun *et al.* 2009	283.3±1.8	25	0.34
Wajilitag	283.0±2.1	Olivine-clinopyroxenite	SIMS	This paper		17	0.33
Piqiang	261.7±1.8	Leucogabbro	LA-ICP-MS	Zhang & Zou 2013	261.7±1.8	20	0.14
Piqiang	262.3±2.1	Gabbro	LA-ICP-MS	Zhang & Zou 2013	262.3±2.1	20	0.6
Halajun 3	268.6±1.5	Granite	LA-ICP-MS	Zhang & Zou 2013	268.6±2.0	15	1.6
Halajun 4	268.8±1.7	Granite	LA-ICP-MS	Zhang & Zou 2013	268.7±1.6	16	0.94
Kezi'ertuo	272.7±1.1	Granite	LA-ICP-MS	Huang *et al.* 2012	272.7±1.1	35	0.74
Halajun 1	278±3	Granite	SHRIMP	C.L. Zhang *et al.* 2010	274.6±2.2	12	1.1
YM30-1	290.9±4.1	Rhyolite	LA-ICP-MS	Tian *et al.* 2010	290.9±4.1	18	1.62
YM5-8	286.6±3.3	Dacite	LA-ICP-MS	Tian *et al.* 2010	286.6±3.3	16	1.04
YM16-1	282.9±2.5	Rhyolite	LA-ICP-MS	Tian *et al.* 2010	282.9±2.5	32	1.26
MN1-1	271.7±2.2	Rhyolite	LA-ICP-MS	Tian *et al.* 2010	271.7±2.2	35	1.08

n, number of dating points used to yield the weight mean average age.

rocks are associated with most continental LIPs (Bryan *et al.* 2002; Bryan 2007), and can predate, be coincident with, or postdate the main phase of basalt magmatism (Bryan *et al.* 2002; Ernst 2014). Based on our new database, the silicic magmatism in Tarim province temporally overlaps with the first pulse of the mafic magmatism (Fig. 7).

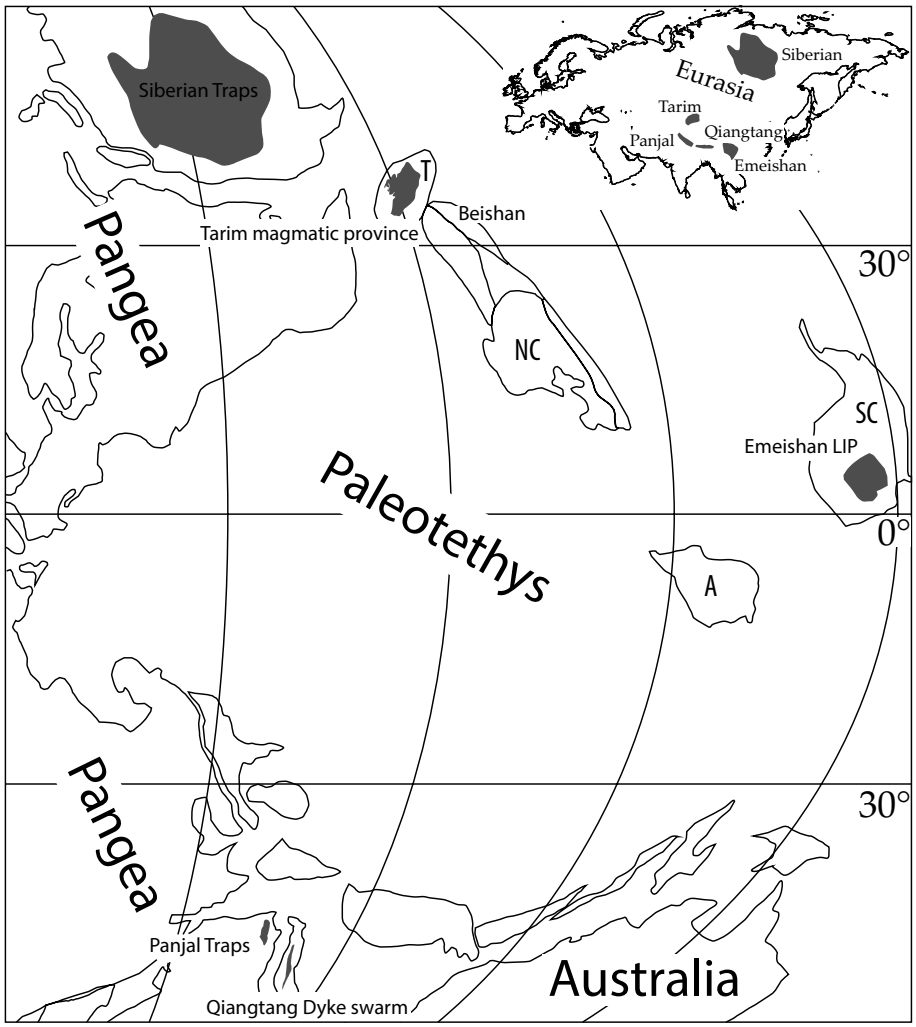

Fig. 8. Palaeogeographical reconstruction at 290 Ma (early Permian) showing simplified plate boundaries and labels of some major features. Continental units: A, Annamia; NC, North China; SC, South China; T, Tarim, modified after Shellnutt *et al.* (2011), Zhai *et al.* (2013), Domeier & Torsvik (2014) and Xiao *et al.* (2014). The dark areas show the recognized LIP-scale or sub-LIP-scale magmatic provinces between 300 and 250 Ma. Small map in the upper right corner shows the present-day positions of these magmatic provinces.

Is the Permian Tarim magmatic province an LIP?

Large igneous provinces are commonly defined by area and volume, as well as duration of magmatism: >100 000 km^2, 100 000 km^3 and a maximum lifespan of up to 50 myr, respectively (Bryan & Ernst 2008; Ernst 2014). The estimates for current Tarim areal extent range from 150 000 km^2 (Chen *et al.* 1997*a*,*b*) to 265 000 km^2, with a volume of 40 000 km^3, based on surface exposures and subsurface seismic and drill core data (Pan 2011; Pan *et al*. 2013). These estimates ignore the effect of erosion and the intrusive component of the province, as well as pyroclastic deposits and silicic lavas. Mafic layered intrusions exposed in NW Tarim indicate that there may have been extensive erosion of surface deposits. There are no available volume estimates for Tarim intrusions, and their equivalent in other LIPs can be volumetrically significant (e.g. the Dufek complex in the Ferrar LIP is 60 000 km^3, Elliot *et al.* 1999).

Pre-Mesozoic LIPs can be intensely fragmented by continental break-up such that portions of a single LIP are dispersed on different crustal blocks (Ernst 2014), and Tarim may represent a remnant of an LIP, similar to the Coppermine River basalts in Canada (Baragar *et al.* 1996). In central Asia there are three mafic provinces with similar ages: the Panjal traps in northern India (*c*. 290 Ma, Shellnutt *et al.* 2011, 2014), Qiangtang dyke swarm in Tibet (*c*. 283 Ma; Zhu *et al*. 2010; Zhai *et al.* 2013), and mafic–ultramafic intrusions (284.0 ± 2.0 to 278.6 ± 1.2 Ma, Qin *et al.* 2011) in the Beishan accretionary belt. The Panjal and Qiangtang provinces are roughly coeval with early Tarim mafic magmatism; however, Permian palaeogeography suggests that they are not likely to be cogenetic, given that they are separated by the Palaeotethys at *c*. 290 Ma (Fig. 8; Domeier & Torsvik 2014). Instead, the approximately coeval mafic–ultramafic intrusions (284.0 ± 2.0 to 278.6 ± 1.2 Ma; Qin *et al.* 2011; Xiao *et al*. 2014) in the Beishan accretionary belt may potentially relate to the Tarim magmatic province, given they were adjacent in the early Permian (Fig. 8).

Conclusions

(1) The new SIMS U–Pb zircon dating of the Halahatang trachydacite layer constrains the youngest emplacement age of the basalt to be 287.2 ± 2.0 Ma in the northern Tarim. The olivine clinopyroxenite from the Wajilitag layered intrusion constrains the crystallization age of the layered intrusion to be 283.2 ± 2.0 Ma.

(2) One hundred and eighteen published geochronological ages were evaluated. Twenty-four of them are robust, including our two new ages.

(3) Two mafic magmatic pulses can be recognized in the province: (a) the Halahatang basalt (>287.2 ± 2.0 Ma) and the Wajilitag layered intrusion (283.2 ± 2.0 Ma); (b) the upper KZ basalt (<267.0 ± 3.4 Ma) and the Piqiang complex (267.0 ± 3.4 Ma).

(4) The silicic magmatism spans at least 20 myr, from 290.9 ± 4.1 to 271.7 ± 2.2 Ma, and temporally overlaps with the first pulse of mafic magmatism.

(5) At the current stage of knowledge, the Tarim magmatic province is of insufficient volume to qualify as an LIP based on the criteria of Ernst (2014). The coeval mafic–ultramafic intrusions in the Beishan accretionary belt may potentially relate to the Tarim magmatic province. Inclusion of silicic volcanic rocks and intrusive

complexes, plus more accurate estimates of erosion, will all increase the estimated original emplacement volume.

Acknowledgements and Funding

Our ideas on re-evaluating the Tarim magmatism geochronology have been stimulated through discussions with numerous colleagues, including D. Peate, A. K. Baksi, W. McClelland, C. Sarkar, E. B. Watson, B. Schoene and R. E. Ernst. Reviews by T. Rooney, A. Marzoli and one anonymous referee are acknowledged. We also thank S. Huang and Y. Pan for providing the drill well information. This study is supported by research grants from the National Basic Research Program of China (2011CB808906) and a GIGCAS 135 project (Y234051001). I.U.P. acknowledges support from NSF MRI EAR 1126728, International Programs and Earth and Environmental Sciences, University of Iowa. W.T. acknowledges support from NSFC grant (41272368).

Scientific editing by Tyrone Rooney

References

Abbott, D.H. & Isley, A.E. 2002. Extraterrestrial influences on mantle plume activity. *Earth and Planetary Science Letters*, **205**, 53–62.

Baksi, A.K. 2003. Critical evaluation of $^{40}Ar/^{39}Ar$ ages for the central Atlantic magmatic province: Timing, duration and possible migration of magmatic centers. *In*: Hames, W.E., McHone, J.G., Renne, P.R. & Ruppel, C. (eds) *The Central Atlantic Magmatic Province: Insights from Fragments of Pangaea*. American Geophysical Union, Geophysical Monograph, **136**, 77–90.

Baksi, A.K. 2007*a*. A quantitative tool for detecting alteration in undisturbed rocks and minerals—I: Water, chemical weathering and atmospheric argon. *In*: Foulger, G.R. & Jurdy, D.M. (eds) *Plates, Plumes and Planetary Processes*. Geological Society of America, Special Papers, **430**, 285–303.

Baksi, A.K. 2007*b*. A quantitative tool for detecting alteration in undisturbed rocks and minerals—II: Application to argon ages related to hotspots. *In*: Foulger, G.R. & Jurdy, D.M. (eds) *Plates, Plumes and Planetary Processes*. Geological Society of America, Special Papers, **430**, 305–333.

Baksi, A.K. 2014. The Deccan Trap–Cretaceous–Paleogene boundary connection; new $^{40}Ar/^{39}Ar$ ages and critical assessment of existing argon data pertinent to this hypothesis. *Journal of Asian Earth Sciences*, **84**, 9–23.

Baragar, W.R.A., Ernst, R.E., Hulbert, L. & Peterson, T. 1996. Longitudinal petrochemical variation in the Mackenzie dyke swarm, northwestern Canadian Shield. *Journal of Petrology*, **37**, 317–359.

Beyer, C., Berndt, J., Tappe, S. & Klemme, S. 2013. Trace element partitioning between perovskite and kimberlite to carbonatite melt: New experimental constraints. *Chemical Geology*, **353**, 132–139.

Boehnke, P., Watson, E.B., Trail, D., Harrison, T.M. & Schmitt, A.K. 2013. Zircon saturation re-revisited. *Chemical Geology*, **351**, 324–334.

Brown, E.R. & Gehrels, G.E. 2007. Detrital zircon constraints on terrane ages and affinities and timing of orogenic events in the San Juan Islands and North Cascades, Washington. *Canadian Journal of Earth Sciences*, **44**, 1375–1396.

Bryan, S.E. 2007. Silicic Large Igneous Provinces. *Episodes*, **30**, 20–31.

Bryan, S.E. & Ernst, R.E. 2008. Revised definition of Large Igneous Provinces (LIPs). *Earth-Science Review*, **86**, 175–202.

Bryan, S.E., Riley, T.R., Jerram, D.A., Stephens, C.J. & Leat, P.T. 2002. Silicic volcanism: An undervalued component of large igneous provinces and volcanic rifted margins. *In*: Menzies, M.A., Klemperer, S.L., Ebinger, C.J. & Baker, J. (eds) *Volcanic Rifted Margins*. Geological Society of America, Special Papers, 97–118.

Bryan, S.E., Ferrari, L., Reiners, P.W., Allen, C.M., Petrone, C.M., Ramos-Rosique, A. & Campbell, I.H. 2008. New insights into crustal contributions to large-volume rhyolite generation in the mid-Tertiary Sierra Madre Occidental province, Mexico, revealed by U–Pb geochronology. *Journal of Petrology*, **49**, 47–77.

Cao, J., Wang, Y.C., Xing, C.M. & Xu, Y.G. 2013. Origin of the early Permian Wajilitag igneous complex and associated Fe–Ti oxide mineralization in the Tarim large igneous province, NW China. *Journal of Asian Earth Sciences*, **84**, 51–68.

Cawthorn, R.G. (ed.). 1996. *Layered Intrusions: Developments in Petrology 15*. Elsevier, Amsterdam.

Chen, H.L., Yang, S.F., Dong, C.W., Jia, C.Z., Wei, G.Q. & Wang, Z.G. 1997*a*. Confirmation of Permian basite zone in Tarim Basin and its tectonic significance. *Geochimica*, **26**(6), 77–87 [in Chinese with English abstract].

Chen, H.L., Yang, S.F., Dong, C.W., Zu, G.Q., Jia, C.Z., Wei, G.Q. & Wang, Z.G. 1997*b*. Geological thermal events in Tarim Basin. *Chinese Science Bulletin*, **42**(7), 580–584.

Chen, N.H., Dong, J.J., Yang, S.F., Chen, J.Y., Li, Z.L. & Ni, N.N. 2014. Restoration of geometry and emplacement mode of the Permian mafic dyke swarms in Keping and its adjacent areas of the Tarim Block, NW China. *Lithos*, **204**, 73–82.

Cohen, K. M., Finney, S. C., Gibbard, P. L., & Fan, J. X. 2013. The ICS international chronostratigraphic chart. *Episodes*, **36**, 199–204.

Courtillot, V.E. & Renne, P.R. 2003. On the ages of flood basalt events. *Comptes Rendus Géoscience*, **335**, 113–140.

Dickinson, W.R. & Gehrels, G.E. 2009. Use of U–Pb ages of detrital zircons to infer maximum depositional ages of strata: A test against a Colorado Plateau Mesozoic database. *Earth and Planetary Science Letters*, **288**, 115–125.

Domeier, M. & Torsvik, T.H. 2014. Plate tectonics in the late Paleozoic. *Geoscience Frontiers*, **5**, 303–350.

Duncan, R.A., Hooper, P.R., Rehacek, J., Marsh, J.S. & Duncan, A.R. 1997. The timing and duration of the Karoo igneous event, southern Gondwana. *Journal of Geophysical Research (Solid Earth)*, **102**, 18127–18138.

Elliot, D.H., Fleming, T.H., Kyle, P.R. & Foland, K.A. 1999. Long-distance transport of magmas in the Jurassic Ferrar large igneous province, Antarctica. *Earth and Planetary Science Letters*, **167**, 89–104.

Ernst, R.E. 2014. *Large Igneous Provinces*. Cambridge University Press, Cambridge.

Ernst, R.E. & Buchan, K.L. 2002. Maximum size and distribution in time and space of mantle plumes: Evidence from large igneous provinces. *Journal of Geodynamics*, **34**, 309–342.

Ernst, R.E., Head, J.W., Parfitt, E., Grosfils, E. & Wilson, L. 1995. Giant radiating dyke swarms on Earth and Venus. *Earth-Science Reviews*, **39**, 1–58.

Gao, Y.S. 2007. Geological characteristics of Wajilitag vanadic titanomagnetite deposit and its prospecting recommendations. *Xinjiang Iron and Steel*, **102**, 8–9. [in Chinese]

Grimes, C.B., John, B.E., Cheadle, M.J., Mazdab, F.K., Wooden, J.L., Swapp, S. & Schwartz, J.J. 2009. On the occurrence, trace element geochemistry, and crystallization history of zircon from *in situ* ocean lithosphere. *Contributions to Mineralogy and Petrology*, **158**, 757–783.

Heaman, L.M. 1989. The nature of the subcontinental mantle from Sr–Nd–Pb isotopic studies on kimberlitic perovskite. *Earth and Planetary Science Letters*, **92**, 323–334.

Heaman, L.M. & Kjarsgaard, B.A. 2000. Timing of eastern North American kimberlite magmatism: Continental extension of the Great Meteor hotspot track? *Earth and Planetary Science Letters*, **178**, 253–268.

Huang, H., Zhang, Z.C., Kusky, T., Santosh, M., Zhang, S., Zhang, D.Y., Liu, J.L. & Zhao, Z.D. 2012. Continental vertical growth in the transitional zone between South Tianshan and Tarim, western Xinjiang, NW China: Insight from the Permian Halajun A1-type granitic magmatism. *Lithos*, **155**, 49–66.

Jia, C.Z. 1997. *Tectonic Characteristics and Oil–Gas, Tarim Basin*. Petroleum Industry Press, Beijing [in Chinese].

Kaczmarek, M.A., Müntener, O. & Rubatto, D. 2008. Trace element chemistry and U–Pb dates of zircons from oceanic gabbros and their relationship with whole rock composition (Lanzo, Italian Alps). *Contributions to Mineralogy and Petrology*, **155**, 295–312.

Katayama, I., Muko, A. *et al*. 2003. Dating of zircon from Ti-clinohumite-bearing garnet peridotite: Implication for timing of mantle metasomatism. *Geology*, **31**, 713–716.

Li, C.N., Lu, F.X. & Chen, M.H. 2001. Research on petrology of the Wajilitag complex body in north edge in the Tarim Basin. *Xinjiang Geology*, **19**, 38–43 [in Chinese with English abstract].

Li, H.Y., Huang, X.L., Li, W.X., Cao, J., He, P.L. & Xu, Y.G. 2013. Age and geochemistry of the Early Permian basalts from Qimugan in the southwestern Tarim basin. *Acta Petrologica Sinica*, **29**, 3353–3368 [in Chinese with English abstract].

Li, X.H., Liu, Y., Li, Q.L., Guo, C.H. & Chamberlain, K.R. 2009. Precise determination of Phanerozoic zircon Pb/Pb age by multicollector SIMS without external standardization. *Geochemistry, Geophysics, Geosystems*, **10**, Q06011.

Li, Y., Su, W. *et al*. 2007. Zircon U–Pb ages of the Early Permian magmatic rocks in the Tazhong–Bachu region, Tarim Basin by LA-ICP-MS. *Acta Petrologica Sinica*, **23**, 1097–1107 [in Chinese with English abstract].

Li, Y.Q., Li, Z.L., Sun, Y.L., Chen, H.L., Yang, S.F. & Yu, X. 2010. PGE and geochemistry of Wajilitag ultramafic cryptoexplosive brecciated rocks from Tarim Basin: Implications for petrogenesis. *Acta Petrologica Sinica*, **26**, 3307–3318 [in Chinese with English abstract].

Li, Z.L., Chen, H.L., Song, B., Li, Y.Q., Yang, S.F. & Yu, X. 2011. Temporal evolution of the Permian large igneous province in Tarim Basin, Northwest China. *Journal of Asian Earth Sciences*, **42**, 917–927.

Li, Z.X., Li, X.H., Kinny, P.D., Wang, J., Zhang, S. & Zhou, H. 2003. Geochronology of Neoproterozoic syn-rift magmatism in the Yangtze Craton, South China and correlations with other continents: Evidence for a mantle super plume that broke up Rodinia. *Precambrian Research*, **122**, 85–109.

Liu, H.Q., Xu, Y.G., Tian, W., Zhong, Y.T., Mundil, R., Li, X.H. & Shangguan, S.M. 2014. Origin of two types of rhyolites in the Tarim Large Igneous Province: Consequences of incubation and melting of a mantle plume. *Lithos*, **204**, 59–72.

Liu, Y.L., Hu, X.F. *et al*. 2012. $^{40}Ar–^{39}Ar$ geochronology and geochemistry of the volcanic rocks from the west segment of Tabei uplift, Tarim Basin. *Acta Petrologica Sinica*, **28**, 2423–2434 [in Chinese with English abstract].

Lu, S.N., Zhao, G.C., Wang, H.C. & Hao, G.J. 2008. Precambrian metamorphic basement and sedimentary cover of the North China Craton: A review. *Precambrian Research*, **160**, 77–93.

Ludwig, K.R. 2008. *Isoplot 3.6*. Berkeley Geochronology Center Special Publications, **4**.

Marzoli, A., Renne, P.R., Piccirillo, E.M., Ernesto, M., Bellieni, G. & De Min, A. 1999. Extensive 200-million year old continental flood basalts of the Central Atlantic Magmatic Province. *Science*, **284**, 616–618.

Mattinson, J.M. 2005. Zircon U–Pb chemical abrasion ('CA-TIMS') method: Combined annealing and multi-step partial dissolution analysis for improved precision and accuracy of zircon ages. *Chemical Geology*, **220**, 47–66.

Miller, J.S., Matzel, J.E., Miller, C.F., Burgess, S.D. & Miller, R.B. 2007. Zircon growth and recycling during the assembly of large, composite arc plutons. *Journal of Volcanology and Geothermal Research*, **167**, 282–299.

Pan, Y. 2011. *The recognition and spatial distribution of Permian igneous in Tarim Basin—Based on logging and seismic technology*. PhD dissertation, Peking University, Beijing [in Chinese with English summary].

Pan, Y., Pan, M., Tian, W., Wang, Z.X., Guan, P., Liu, X. & Pan, W.Q. 2013. Redefined distribution of the Permian basalt in the central Tarim Area: A new approach based on down hole logging data explanation. *Acta Geologica Sinica*, **87**, 1542–1550 [in Chinese with English abstract].

Polat, A., Frei, R., Fryer, B. & Appel, P.W. 2009. The origin of geochemical trends and Eoarchean (*ca*. 3700 Ma) zircons in Mesoarchean (*ca*. 3075 Ma) ocelli-hosting pillow basalts, Ivisaartoq greenstone belt, SW Greenland: Evidence for crustal contamination versus crustal recycling. *Chemical Geology*, **268**, 248–271.

Prokoph, A., Ernst, R.E. & Buchan, K.L. 2004. Time-series analysis of large igneous provinces: 3500 Ma to present. *Journal of Geology*, **112**, 1–22.

Qin, K.Z., Su, B.X. *et al*. 2011. SIMS zircon U–Pb geochronology and Sr–Nd isotopes of Ni–Cu-bearing mafic–ultramafic intrusions in eastern Tianshan and Beishan in correlation with flood basalts in Tarim Basin (NW China): Constraints on a *ca*. 280 Ma mantle plume. *American Journal of Science*, **311**, 237–260.

Riishuus, M.S., Peate, D.W., Tegner, C., Wilson, J.R., Brooks, C.K. & Harris, C. 2006. Temporal evolution of a long-lived syenitic centre: The Kangerlussuaq Alkaline Complex, East Greenland. *Lithos*, **92**, 276–299.

Rui, X.J., He, J.R. & Guo, K.Y. 2002. *Mineral Resources of Tarim Block*. Geological Publishing House, Beijing, 56–157 [in Chinese with English abstract].

Sarkar, C., Storey, C.D., Hawkesworth, C.J. & Sparks, R.S.J. 2011. Degassing in kimberlite: Oxygen isotope ratios in perovskites from explosive and hypabyssal kimberlites. *Earth and Planetary Science Letters*, **312**, 291–299.

Saunders, A.D., Fitton, J.G., Kerr, A.C., Norry, M.J. & Kent, R.W. 1997. The north Atlantic igneous province. *In*: Mahoney, J.J. & Coffin, M.L. (eds) *Large Igneous Provinces: Continental, Oceanic, and Planetary Flood Volcanism*. American Geophysical Union, Geophysical Monograph, **100**, 45–93.

Schärer, U., Berndt, J. & Deutsch, A. 2011. The genesis of deep-mantle xenocrystic zircon and baddeleyite megacrysts (Mbuji–Mayi kimberlite): Trace-element patterns. *European Journal of Mineralogy*, **23**, 241–255.

Schmitz, M.D. & Schoene, B. 2007. Derivation of isotope ratios, errors, and error correlations for U–Pb geochronology using ^{205}Pb–^{235}U–(^{233}U)-spiked isotope dilution thermal ionization mass spectrometric data. *Geochemistry, Geophysics, Geosystems*, **8**, Q08006.

Shangguan, S.M., Tian, W., Xu, Y.G., Guan, P. & Pan, L. 2012. The eruption characteristic of the Tarim flood basalt. *Acta Petrologica Sinica*, **38**, 8–20 [in Chinese with English abstract].

Shangguan, S.M. 2015. *Volcanostratigraphy, geochronology and geochemistry of flood basalt volcanism in the Tarim magmatic province*. PhD dissertation, Guangzhou Institute of Geochemistry, Guangzhou [in Chinese with English summary].

Sharp, W.D. & Clague, D.A. 2006. 50-Ma initiation of the Hawaiian–Emperor Bend records major change in Pacific plate motion. *Science*, **313**, 1281–1284.

Shellnutt, J.G., Bhat, G.M., Brookfield, M.E. & Jahn, B.M. 2011. No link between the Panjal Traps (Kashmir) and the Late Permian mass extinctions. *Geophysical Research Letters*, **38**, L19308.

Shellnutt, J.G., Bhat, G.M., Wang, K.L., Brookfield, M.E., Jahn, B.M. & Dostal, J. 2014. Petrogenesis of the flood basalts from the Early Permian Panjal Traps, Kashmir, India: Geochemical evidence for shallow melting of the mantle. *Lithos*, **204**, 159–171.

Sláma, J., Košler, J. *et al*. 2008. Plešovice zircon—a new natural reference material for U–Pb and Hf isotopic microanalysis. *Chemical Geology*, **249**, 1–35.

Sparks, R. 2013. Kimberlite volcanism. *Annual Review of Earth and Planetary Sciences*, **41**, 497–528.

Stacey, J.S. & Kramers, J.D. 1975. Approximation of terrestrial lead isotope evolution by a two-stage model. *Earth and Planetary Science Letters*, **26**, 207–221.

Sun, L.H., Wang, Y.J., Fan, W.M. & Zi, J.W. 2008. A further discussion of the petrogenesis and tectonic implication of the Mazhashan syenites in the Bachu area. *Journal of Jilin University (Earth Science Edition)*, **38**, 8–20 [in Chinese with English abstract].

Sun, Y., Xiao, Y.F., Zhao, X.K., Qian, Y.X., Xiao, G.W. & Liu, H.Q. 2009. The zircon U-Pb age of Mazha'erTage alkalic complex in the Tarim Basin and its geologic significance. *Acta Geologica Sinica*, **83**, 775-781 [in Chinese with English abstract].

Tian, W., Campbell, I.H. *et al*. 2010. The Tarim picrite–basalt–rhyolite suite, a Permian flood basalt from northwest China with contrasting rhyolites produced by fractional crystallization and anatexis. *Contributions to Mineralogy and Petrology*, **160**, 407–425.

Wei, X. & Xu, Y.G. 2011. Petrogenesis of Xiaohaizi syenite complex from Bachu area, Tarim. *Acta Petrologica Sinica*, **27**, 2984–3004 [in Chinese with English abstract].

Wei, X. & Xu, Y.G. 2013. Petrogenesis of the mafic dykes from Bachu and implications for the magma evolution of the Tarim large igneous province, NW China. *Acta Petrologica Sinica*, **29**, 3323–3335 [in Chinese with English abstract].

Wei, X., Xu, Y.G., Feng, Y.X. & Zhao, J.X. 2014. Plume -lithosphere interaction in the generation of the Tarim large igneous province, NW China: geochronological and geochemical constraints. *American Journal of Science*, **314**, 314–356.

Wiedenbeck, M., Alle, P. *et al*. 1995. Three natural zircon standards for U–Th–Pb, Lu–Hf, trace-element and REE analyses. *Geostandards Newsletter*, **19**, 1–23.

Xiao, W.J., Han, C.M. *et al*. 2014. How many sutures in the southern Central Asian Orogenic Belt: Insights from East Xinjiang–West Gansu (NW China)? *Geoscience Frontiers*, **5**, 525–536.

Xu, Y.G., Wei, X., Luo, Z.Y., Liu, H.Q. & Cao, J. 2014. The Early Permian Tarim Large Igneous Province: Main characteristics and a plume incubation model. *Lithos*, **204**, 20–35.

Yang, S.F., Li, Z.L., Chen, H.L., Chen, W. & Yu, X. 2006. ^{40}Ar/^{39}Ar dates of basalts from Tarim Basin, NW China and its implication to a Permian thermal tectonic event. *Journal of Zhejiang University—Science A*, **7**, 170–174.

Yang, S.F., Li, Z.L. & Chen, H.L. 2007. Permian bimodal dyke of Tarim Basin, NW China: Geochemical characteristics and tectonic implications. *Gondwana Research*, **12**, 113–120.

Yang, S.F., Chen, H.L., Li, Z.L., Li, Y.Q., Yu, X., Li, D.X. & Meng, L.F. 2013. Early Permian Tarim Large Igneous Province in northwest China. *Science China—Earth Sciences*, **56**, 2015–2026.

Yu, J.C., Mo, X.X., Dong, G.C., Yu, X.H., Xing, F.C., Li, Y. & Huang, X.K. 2011*a*. Felsic volcanic rocks from northern Tarim, NW China: Zircon U-Pb dates and geochemical characteristics. *Acta Petrologica Sinica*, **27**, 2184–2194 [in Chinese with English abstract].

Yu, X., Yang, S.F., Chen, H.L., Chen, Z.Q., Li, Z.L., Batt, G.E. & Li, Y.Q. 2011*b*. Permian flood basalts from the Tarim Basin, Northwest China: SHRIMP zircon U–Pb dates and geochemical characteristics. *Gondwana Research*, **20**, 485–497.

Zhai, Q.G., Jahn, B.M. *et al*. 2013. The Carboniferous ophiolite in the middle of the Qiangtang terrane, Northern Tibet: SHRIMP U–Pb dating, geochemical and Sr–Nd–Hf isotopic characteristics. *Lithos*, **168**, 186–199.

Zhang, S.B. 2003. A Guide to the Stratigraphic Investigation on the Periphery of the Tarim Basin. *Petroleum Industry Press*, 280 [in Chinese].

Zhang, C.L. & Zou, H.B. 2013. Permian A-type granites in Tarim and western part of Central Asian Orogenic Belt (CAOB): Genetically related to a common Permian mantle plume? *Lithos*, **172**, 47–60.

Zhang, C.L., Li, X.H., Li, Z.X., Ye, H.M. & Li, C.N. 2008. A Permian layered intrusive complex in the Western Tarim Block, northwestern China: Product of a *ca*. 275-Ma mantle plume? *Journal of Geology*, **116**, 269–287.

Zhang, C.L., Xu, Y.G., Li, Z.X., Wang, H.Y. & Ye, H.M. 2010. Diverse Permian magmatism in the Tarim Block, NW China: Genetically linked to the Permian Tarim mantle plume? *Lithos*, **119**, 537–552.

Zhang, D.Y., Zhou, T.F., Yuan, F., Fan, Y., Liu, S. & Du, H.X. 2010. LA-ICPMS U–Pb ages, Hf isotope characteristics of zircons from basalts in the Kupukuziman Formation, Keping area, Tarim Basin. *Acta Petrologica Sinica*, **26**, 963–974 [in Chinese with English abstract].

Zhang, D.Y., Zhou, T.F., Yuan, F., Jowitt, S.M., Fan, Y. & Liu, S. 2012. Source, evolution and emplacement of Permian Tarim Basalts: Evidence from U–Pb dates, Sr–Nd–Pb–Hf isotope systematics and whole rock geochemistry of basalts from the Keping area, Xinjiang Uygur Autonomous region, northwest China. *Journal of Asian Earth Sciences*, **49**, 175–190.

Zhang, D.Y., Zhang, Z.C., Santosh, M., Cheng, Z., He, H. & Kang, J. 2013. Perovskite and baddeleyite from kimberlitic intrusions in the Tarim large igneous province signal the onset of an end-Carboniferous mantle plume. *Earth and Planetary Science Letters*, **361**, 238–248.

Zhang, H.A., Li, Y.J. *et al*. 2009. Isotopic geochronology of Permian igneous rocks in the Tarim Basin. *Chinese Journal of Geology*, **44**, 137–158 [in Chinese with English abstract].

Zhang, Z.L., Qin, Q.M., Tian, W., Cao, B., Li, B.S. & Chen, M.M. 2008. Emplacement characteristics and spatial distribution of Permian Mazhartager basic dike swarms in Bachu area, Tarim basin. *Acta Petrologica Sinica*, **24**, 2273–2280 [in Chinese with English abstract].

Zhou, M.F., Zhao, J.H., Jiang, C.Y., Gao, J.F., Wang, W. & Yang, S.H. 2009. OIB-like, heterogeneous mantle sources of Permian basaltic magmatism in the western Tarim Basin, NW China: Implications for a possible Permian large igneous province. *Lithos*, **113**, 583–594.

Zhu, D.C., Mo, X.X. *et al*. 2010. Presence of Permian extension- and arc-type magmatism in southern Tibet: Paleogeographic implications. *Geological Society of America Bulletin*, **122**, 979–993.

Zou, S.Y., Li, Z.L. *et al*. 2013. U–Pb dates and Hf isotopic compositions of the detrital zircons from Permian sedimentary rocks in Keping area of Tarim Basin, Xianjiang, China: Constraints on geological evolution of Tarim Block. *Acta Petrologica Sinica*, **29**, 3369–3388 [in Chinese with English abstract].

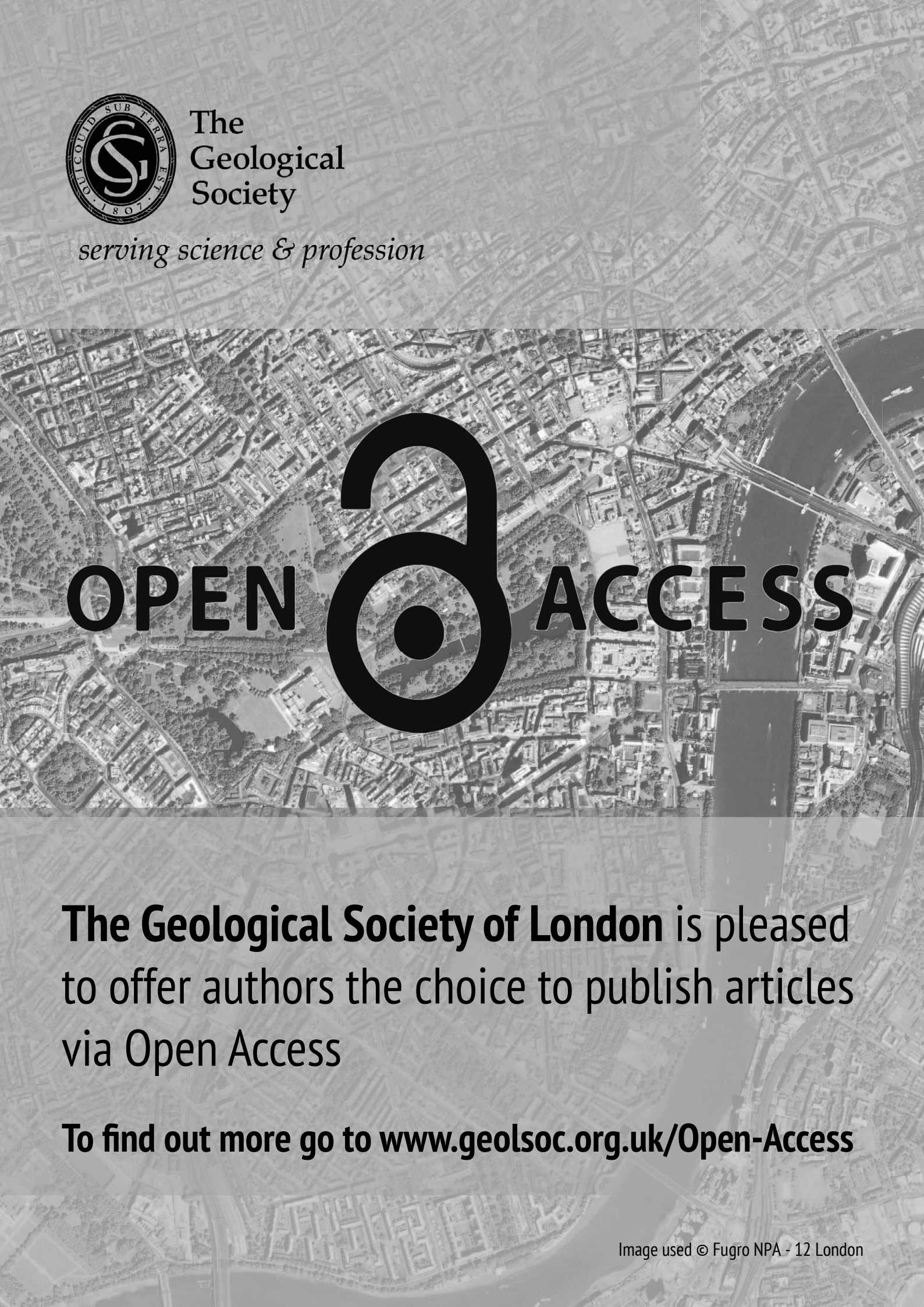
The
Geological
Society
serving science & profession
OPEN ACCESS
The Geological Society of London is pleased
to offer authors the choice to publish articles
via Open Access
To find out more go to www.geolsoc.org.uk/Open-Access
Image used © Fugro NPA - 12 London